Application of the Doublet-Lattice Method to Nonplanar Configurations in Subsonic Flow

T. P. KALMAN,* W. P. RODDEN,† AND J. P. GIESING‡
Douglas Aircraft Company, Long Beach, Calif.

This paper presents a short survey of the more recent developments of the Vortex- and Doublet-Lattice Methods for calculating aerodynamic lift distributions on surfaces in steady and oscillatory motion at subsonic speeds. The methods are outlined and some computational details, not previously documented, are discussed. Correlations are shown for nonplanar configurations by comparing results with solutions obtained by other means, and with experimental data. The nonplanar configurations considered in steady and oscillatory motion include T-tails, wing-pylon combinations, annular wings, wing-fuselage combinations, and wings in ground proximity. The accuracy and versatility of the methods are demonstrated by the extensive correlations obtained on all configurations.

Nomenclature

AR = aspect ratio
b = wing span
C_L = lift coefficient (L/qS)
C_M = moment coefficient ($M/qS\bar{c}$)
C_Y = side force coefficient (Y/qS)
CP = control point location given in percent box length
c = local chord
$\bar{c}$ = reference chord length
c_l = local lift coefficient (l/qS)
D = matrix of normalwash influence coefficients for steady flow
ΔD = matrix of incremental normalwash influence coefficients for oscillatory flow
D/L = ratio of diameter to length
h = height above the ground
k = reduced frequency ($\omega\bar{c}/2U$)
L = lift or body length
l = local lift
M = Mach number; moment
p = lifting pressure coefficient $[(p_{\text{lower}} - p_{\text{upper}})/q]$
q = dynamic pressure
S = wing area
U = freestream velocity
w = normalwash
x,y,z = Cartesian coordinate system
Y = side force
α = angle of attack
γ = dihedral angle
ω = angular frequency

Introduction

DISCRETE vortices for the numerical solution of the steady subsonic lifting surface problem were first used in the Vortex-Lattice Method of Falkner[1] in 1943. At that time, the number of unknowns was kept low by making assumptions on the chordwise and spanwise load distributions. However, the speed and capacity achieved in the past decade by electronic digital computers make such assumptions unnecessary, and a number of direct solutions have been proposed. These new, but similar, independent developments of the Vortex-Lattice Method include the variations of Rubbert,[2] Dulmovits,[3] Hedman,[4] and Belotserkovskii.[5]

An extension of Falkner's method to the oscillatory case was given by Runyan and Woolston[6] using a power series form for the oscillatory kernel of the integral equation, but retaining the assumed loading functions. A number of direct solutions to the oscillatory problem have also been proposed recently to eliminate the use of loading functions and to utilize improved forms of the oscillatory kernel. Among these new developments for discrete loading elements are the variations of Stark,[7] Albano and Rodden,[8] Petkas,[9] and Houbolt.[10] The extension of the Vortex-Lattice Method to the oscillatory case has been called the Doublet-Lattice Method. The only attempt to provide a rigorous analytical basis for the Lattice Methods known to the authors is the investigation of the steady two-dimensional case by James.[11] The adequacy of the Lattice Methods in steady and unsteady three-dimensional cases, however, has been demonstrated by comparison of results with solutions obtained by other means and with experimental data. Previous comparisons have been made, for the most part, for planar surfaces. It is the purpose of this paper to demonstrate the adequacy of the Lattice Methods by further comparisons of interfering and intersecting surfaces for nonplanar configurations.

Vortex- and Doublet-Lattice Methods

The flow singularities used to model the lifting surface are steady horseshoe vortices and oscillatory doublets along the bound vortex. The doublet line is equivalent, at zero frequency, to the horseshoe vortex and thus the horseshoe vortex need not be used. However, since the effects of the vortex system can be analyzed exactly, while the effects of a

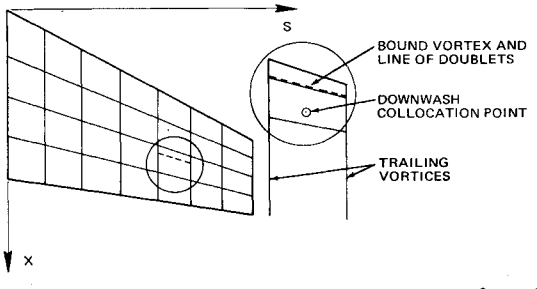

Fig. 1 Surface division into boxes and location of vortices, doublets, and collocation points.

Presented as Paper 70-539 at the AIAA Atmospheric Flight Mechanics Conference, Tullahoma, Tenn., May 13–15, 1970; submitted June 5, 1970; revision received November 2, 1970.

* Engineer/Scientist, Structural Mechanics Section. Member AIAA.
† Consulting Engineer. Associate Fellow AIAA.
‡ Senior Group Engineer, Structural Mechanics Section. Associate Fellow AIAA.

doublet line can only be approximated, improved accuracy is obtained by using both the vortex and doublet systems. In this way, the vortices represent the steady flow effects and the doublets represent the incremental effects of oscillatory motion.

The first step in the idealization is the division of the surface(s) into small trapezoidal elements (boxes) arranged in strips parallel to the freestream so that surface edges, fold lines, and hinge lines lie on box boundaries (Fig. 1). Then, to represent the steady flow effects, a horseshoe vortex is placed on each of the boxes such that the bound vortex to the horseshoe system coincides with the quater-chord line of the box. To represent the oscillatory increment, a distribution of acceleration potential doublets (which have the steady flow doublet strength subtracted) of uniform strength is superimposed on the bound vortex.

The surface boundary condition is a prescribed normalwash (e.g., downwash) applied at the control point of each box. The control point is centered spanwise on the three-quarter chord line of the box (Fig. 1). This choice of control point location, shown by James[11] to be optimum for the two-dimensional case, results in a high degree of accuracy.

The influences of all vortices and doublets (indexed by the subscript j are summed for each control point (indexed by the subscript i) to obtain the total dimensionless normalwash, w_i, at the control point

$$w_i = \Sigma_j(D_{sij} + \Delta D_{ij})p_j \tag{1}$$

In matrix notation for all control points, Eq. (1) becomes

$$\{w\} = [D_s + \Delta D]\{p\} \tag{2a}$$

$$\{w\} = [D]\{p\} \tag{2b}$$

In the Eqs. (2), D_s is the steady downwash factor, ΔD is the complex incremental oscillatory downwash factor, p is the pressure coefficient at the center of the bound vortex, and D is the total downwash factor. The solution of Eqs. (2) (regarded as a system of simultaneous equations, rather than a matrix inversion exercise) for a prescribed distribution of normalwash leads to the solution for the pressure coefficients.

The working equations for the downwash factors for an oblique horseshoe vortex system have been given by Hedman[4] and the equations for the incremental downwash factors for the oscillatory doublet line are obtained from Ref. 8. Additional numerical considerations required for the computer program[12] are discussed in the Appendix.

T-Tails

A T-tail configuration (Fig. 2) that has been analyzed extensively was first analyzed by Stark,[13] and subsequently by Davies[14] and Zwaan.[15] The Vortex- and Doublet-Lattice solutions are compared with their solutions in Tables 1 and 2, respectively. The three modes of motion are 1) yawing about a vertical axis through the center of the root chord of the fin, 2) sideway, and 3 rolling about the fin-stabilizer intersection. The generalized forces are yawing moment, side force, and rolling moment about the same axes. The definitions of the generalized force coefficients are those of Stark.[13]

Table 1 Comparison of static generalized aerodynamic forces calculated by Stark and MDC

Coefficients		M = 0.0	M = 0.8
Stark	Yawing	−0.0990	−0.1295
MDC	moment	−0.0970	−0.1242
Stark	Side	−0.5173	−0.5947
MDC	force	−0.5355	−0.6170
Stark	Rolling	−0.1231	−0.1238
MDC	moment	−0.1255	−0.1258

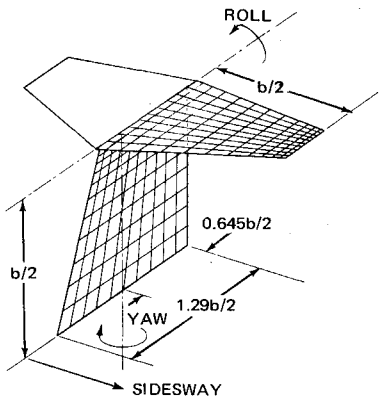

Fig. 2 Aerodynamic idealization of Stark's T-tail.

The horizontal stabilizer has an aspect ratio of 2.84 and a taper ratio of 0.503. The sweep angle of the stabilizer mid-chord line is 8.2°. The height ($b/2$) of the fin is equal to the semispan of the stabilizer, and its mid-chord line is swept 29.5°. The root chord of the fin is $1.29b/2$ and its taper ratio is 0.645. Figure 2 also shows the stabilizer mounted on the fin and the distribution of aerodynamic boxes. The lattice results are seen to agree well within the variations of the other calculations presented in Tables 1 and 2. Experimental data and theoretical results on a practical T-tail model have been reported by Zwaan.[16] The configuration (Fig. 3) has a horizontal stabilizer with aspect ratio of 3.64 and taper ratio§ of 0.5. The sweep angle of the stabilizer mid-chord line is 22.5° and its root chord is 545 mm. The height of the fin is 912.7 mm and its mid-chord line is swept 39°. The root chord of the fin is 1052.5 mm and its taper ratio is 0.85. The stabilizer mounted on the fin and the distribution of aerodynamic boxes are also shown in Fig. 3.

The T-tail was tested in two modes of motion: 1) rolling about an axis parallel to the tunnel wall at 100 mm below the tunnel wall, and 2) yawing about an axis perpendicular to the tunnel wall as shown in Fig. 3. The low-speed wind

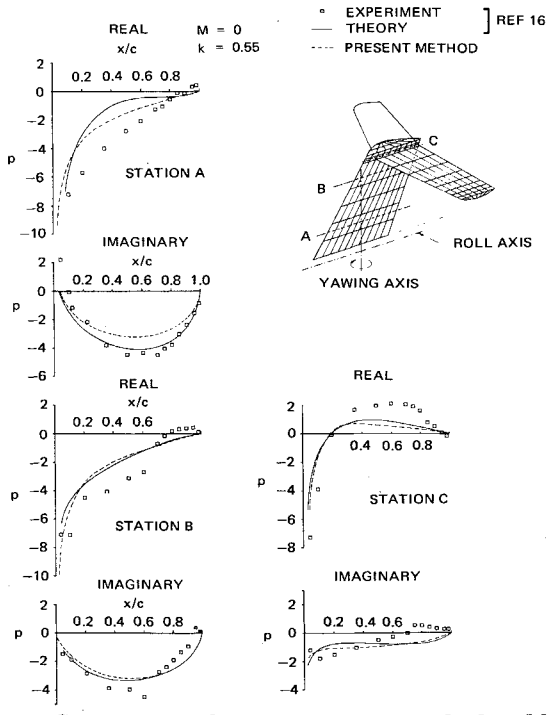

Fig. 3 Comparison of experimental and calculated lifting pressure distribution on T-tail oscillating in yaw (stations A, B, and C).

§ The taper ratio was calculated omitting the rounded parts on both the fin-top and stabilizer tip.

Table 2 Comparison of generalized aerodynamic forces calculated by Davies, Stark, NLR, and MDC ($M = 0.8k$, = 0.2)

Coefficients		Yawing (plus nose right)		Sidesway (plus left)		Rolling (plus right wing down)	
		Re	*Im*	*Re*	*Im*	*Re*	*Im*
Davies		−0.0846	−0.5090	0.0461	−0.0283	0.0141	0.0260
Stark	Yawing	−0.0961	−0.4811	0.0412	−0.0300	0.0125	0.0239
NLR	moment	−0.0922	−0.5155	0.0466	−0.0298	0.0145	0.0259
MDC	(plus nose left)	−0.0837	−0.5270	0.0470	−0.0278	0.0137	0.0257
Davies		−0.6224	−0.3754	0.0265	−0.1234	0.0169	−0.0305
Stark	Side	−0.6108	−0.3625	0.0241	−0.1211	0.0158	−0.0295
NLR	force	−0.6236	−0.3728	0.0260	−0.1236	0.0168	−0.0304
MDC	(plus left)	−0.6270	−0.3965	0.0297	−0.1260	0.0171	−0.0318
Davies		−0.1248	−0.1237	0.0150	−0.0262	0.0179	−0.0502
Stark	Rolling	−0.1247	−0.1151	0.0134	−0.0255	0.0179	−0.0497
NLR	moment	−0.1235	−0.1217	0.0148	−0.0259	0.0179	−0.0502
MDC	(plus right wing down)	−0.1270	−0.1266	0.0154	−0.0269	0.0186	−0.0529

tunnel tests were conducted at reduced frequencies up to 0.55. Comparisons of the present method with the experiment and theory of Ref. 16 were made of the real and imaginary parts of the chordwise pressure distribution in yaw of both the fin and stabilizer for two reduced frequencies (0.55 and 0.35), as shown in Figs. 3 and 4. The agreement between the present method and the experimental data is generally good; however, the agreement between Zwaan's theoretical results and the present method is better.

Wing-Pylon Interference

A simplified steady Vortex-Lattice Method with only one box on the chord was developed by Campbell[17] in 1951 and applied recently by Blackwell[18] to wings with pylons, fences, and end-plates. Correlation with experimental data is also shown in Ref. 18. The experimental data on end-plates reported by Ingelmann-Sundberg[19] are shown, as are data on fences reported by Weber and Lawford.[20] A comparison of Vortex-Lattice results and Blackwell's results with the experimental data is shown in Figs. 5–9.

Figure 5 presents a comparison of span load as calculated by the present method and Blackwell's results for a wing with a pylon in steady flow at zero Mach number. The wing has an aspect ratio of 6.67, a taper ratio of 0.33 and a quarter-chord sweep angle of 30°. The pylon, which is unswept and untapered, lies along the chord at 60% semispan and has a span equal to 20% of the wing semispan. In the present method, the wing is idealized by 14 strips concentrated near the tip, and to a lesser degree, near the root of the wing. The pylon is idealized by 6 equal strips, and all strips are subdivided into 6 equal chordwise boxes, both on the wing and the pylon. The comparison is made with and without the pylon. The two methods are in good agreement even near the wing-pylon intersection. The span load for oscillatory motion is also presented for the wing-pylon combination pitching about the wing apex with a reduced frequency of $k = 0.5$. The real part (in-phase component) is given in the upper curve and the imaginary part (quadrature or out-of-phase component) is given in the lower curve.

Figure 6 presents a comparison of experimental and calculated lift coefficient distribution on a wing with end plates. The wing has an aspect ratio of 4.5, a taper ratio of 0.5, and a quater-chord sweep angle of 40°. The end plates are circular and equal in diameter to the wing tip chord. In the present method, the wing is idealized by 20 strips concentrated near the tip, and to a lesser degree, near the root of the wing. The endplate is idealized by 16 strips concentrated near the "tips" of the endplate. For comparison on the chordwise pressure distribution, each strip is subdivided into 8 chordwise

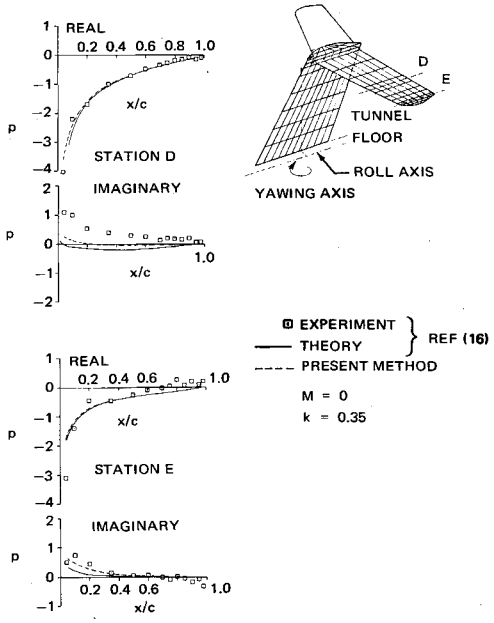

Fig. 4 Comparison of experimental and calculated lifting pressure distribution on T-tail oscillating in yaw (stations D and E).

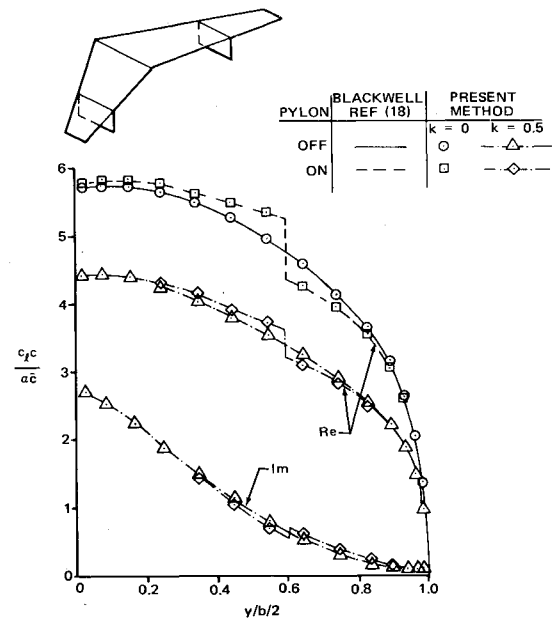

Fig. 5 Comparison of the span load for wing with and without pylons in steady and oscillatory flow.

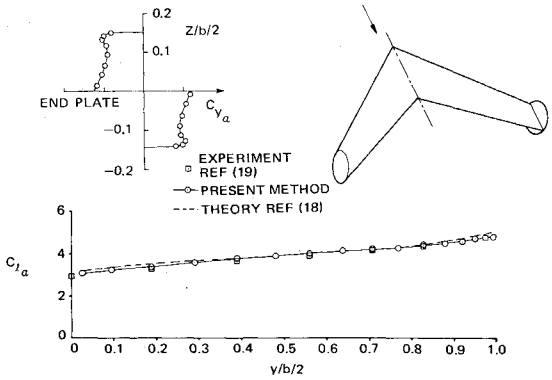

Fig. 6 Comparison of experimental and calculated lift-curve-slope distribution for wing with end plates in steady flow.

boxes concentrated near the leading edge. The wing is in steady flow at a Mach number $M = 0.1$. The experimental data are taken from Ref. 19 while the calculated results are given by Blackwell[18] and the present method. The two calculations are in excellent agreement with each other and with the experimental data. The spanwise side force coefficient distribution on the end plate is also shown in Fig. 6.

Reference 19 gives pressure distribution data for the wing with end plates in addition to lift coefficient data. Figure 7 presents a comparison of calculated results for three wing stations (A, B, and C) at 2.5, 56, and 92% of the semispan, respectively. The agreement between the experimental data and calculated results is generally good with some deviations near the one-quarter chord region of stations B and C. The additional experimental lift that these regions seem to indicate does not appear in the span loads presented in Fig. 6.

Figure 8 presents a comparison of experimental and calculated lift coefficient distribution for a wing with a fence in steady flow at a Mach number of $M = 0.1$. The wing has an aspect ratio of 2.0, a sweep of 45° and no taper except where the curved leading edge wing tips are fitted. The fence lies along the 42% chord of the semispan and extends the full wing chord length. The fence is untapered, unswept, and extends above and below the wing plane to a height of 6% of the wing semi-span (i.e., the span of fence is 12% of the wing semi-span). In the present method, the wing is idealized by 20 strips concentrated near the intersection with the fence and

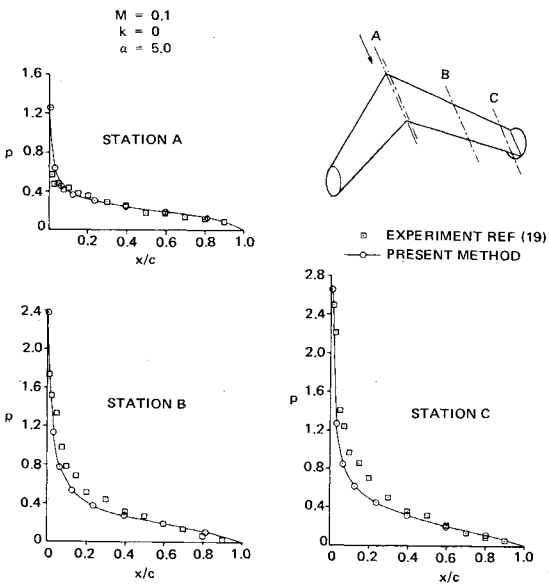

Fig. 7 Comparison of experimental and calculated lifting pressure distributions for three wing stations on wing with end plates.

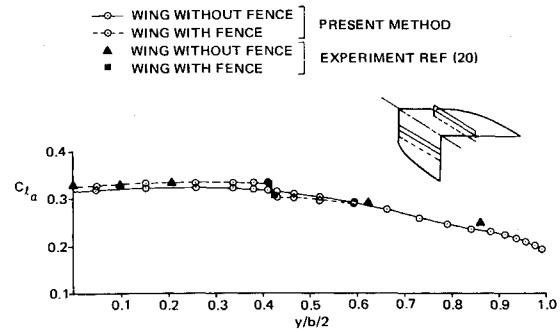

Fig. 8 Comparison of experimental and calculated span load for wing with and without a fence in steady flow.

near the tip of the wing. The fence is idealized by 8 equal strips, and each strip is subdivided into 8 chordwise boxes concentrated near the leading edge. For comparison, calculations for a wing without a fence are also presented in Fig. 8.

The calculations presented in Fig. 8 show excellent agreement with the limited experimental data given in Ref. 20. The two experimental data points were obtained by integrating the pressure distributions just inboard and just outboard of the fence. Figure 9 shows a comparison of these experimental pressure distributions with those obtained using the present method. The agreement between calculated and experimental results is good. Since Blackwell's method does not produce a chordwise loading (its lift is concentrated along the one-quarter chord line), no additional results could be compared.

Annular Wing

A large portion of Belotserkovskii's book[5] is devoted to the analysis of the annular or ring-wing. The Vortex-Lattice Method has been applied to annular wings of varying aspect ratio (i.e., diameter to length ratio D/L) by idealizing the circular cylinder using 24 inscribed equal planar panels (Fig. 10). Each panel is divided into ten equally spaced boxes for the cases: $D/L = 0.8$, 1.0, 1.5, 2.0, and 3.0. For the cases, $D/L = 0.1$ and 0.5, fourteen boxes are used and are concentrated near the leading edge where most of the lift exists (in the limit as $D/L \to 0$, the center of lift is at the leading edge).

In addition to the configuration, Fig. 10 shows a comparison of lift, and moment about the mid-chord point, and pitch rate coefficients as calculated by Belotserkovskii (both exact and slender wing theory) and by the present method. The agreement is excellent.

In addition to the static stability derivatives for angle-of-attack and pitch rate, the stability derivatives for rate of change of angle of attack, $C_{L_{\dot{\alpha}}}$ and $C_{M_{\dot{\alpha}}}$, have been calculated

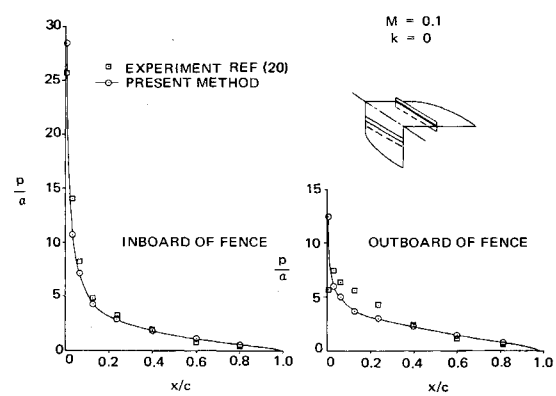

Fig. 9 Comparison of experimental and calculated chordwise load distributions just inboard and just outboard of a fence.

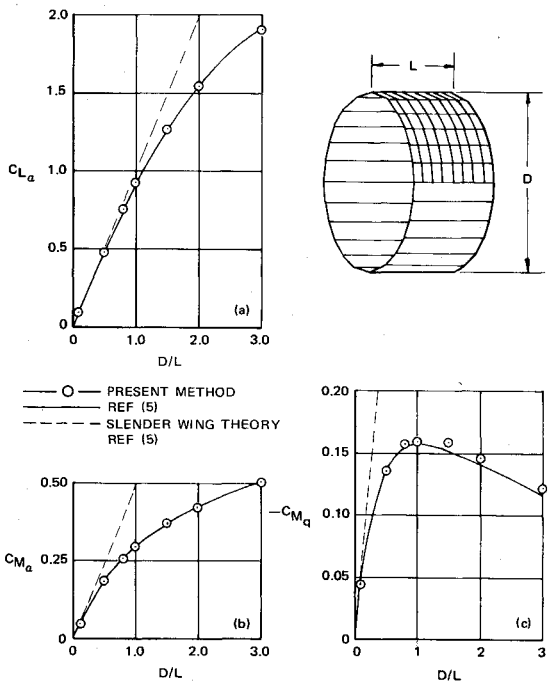

Fig. 10 Static stability derivatives for annular wings of various D/L ratios.

by the Doublet-Lattice Method (Fig. 11). These were calculated from the complex lift and moment coefficients for harmonic pitching with unit amplitude at a low reduced frequency ($k = \omega L/2U = 0.05$) by the method presented in Ref. 22. The slender wing theory of Laschka, Ref. 21, is also shown in Fig. 11 for comparison.

Wing-Fuselage Interference

Giesing[23] and Woodward[24] have developed methods that treat wing-fuselage interference in steady flow. Giesing utilizes a wing image system as well as an axially segmented line doublet within the fuselage to simulate the interference. Woodward, however, uses lifting surface elements on the fuselage surface to obtain a solution. Lifting elements are placed on the fuselage only in the vicinity of the wing. This segment of the fuselage must have a constant diameter. Woodward is, in effect, representing the fuselage by an annular wing. The accuracy of representing a fuselage by an annular wing is not thoroughly investigated here; however, pertinent information is presented in the following paragraphs.

Figure 12 presents a comparison of wing span load (or lift coefficient since the wing chord length is constant) for a wing-

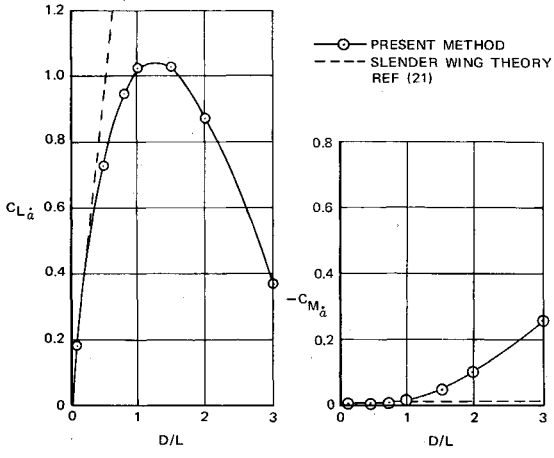

Fig. 11 Dynamic stability derivatives for annular wings of various D/L ratios.

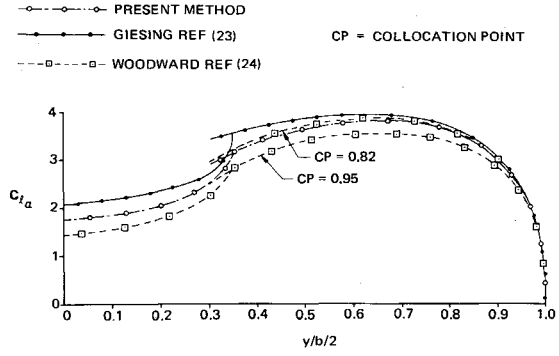

Fig. 12 Span load across the wing and fuselage.

fuselage combination in steady flow $M = 0.8$, as calculated by the present method and the methods in Refs. 23 and 24. The wing alone is given an angle of attack; the fuselage is aligned with the flow. The configuration considered and its sub-element, or box distribution, are shown in Fig. 13. A constant chord, 45° swept wing is attached to an annular wing whose aspect ratio is $D/L = 1/3.8$. The half-span of the exposed wing is equal to the diameter of the annular wing.

Unlike the present method, Woodward's method requires that the collocation points of the lifting surface elements be specified. It is suggested in Ref. 24 that the collocation point (CP) be located near the trailing edge of each box or element, specifically, at 95% on each element. When the 95% point is used, the chordwise and spanwise load distribu-

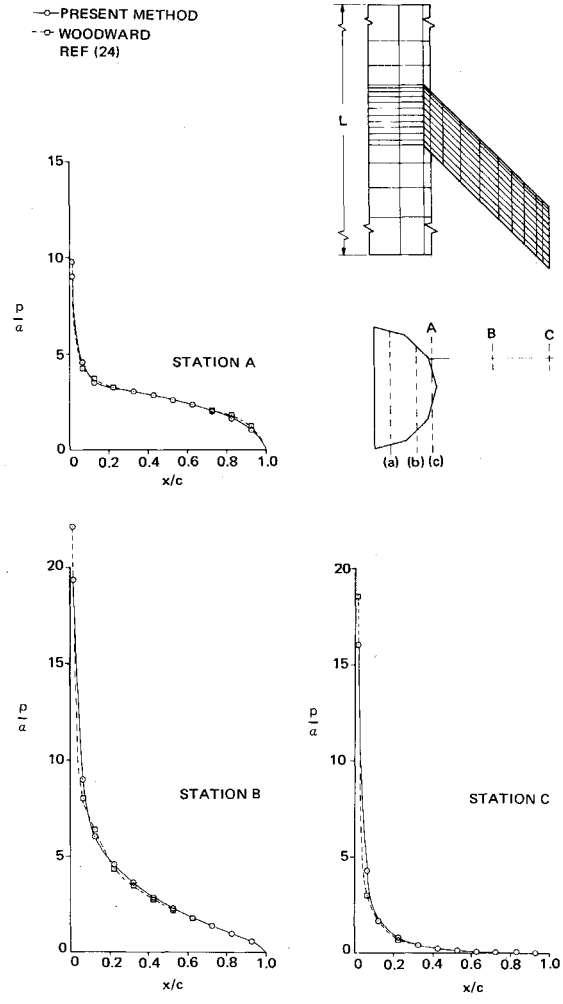

Fig. 13 Lifting pressure distributions at three wing stations.

tions fall considerably below both the present method and that in Ref. 23. Two other locations were tried: 97.5% and 82%. The results are in very good agreement at the 82% point. Subsequent to these calculations, an investigation was made by James[25] on the optimum location of the *CP* in the two-dimensional case for the Woodward approach. His results indicate that for uncambered surfaces, such as considered here, the *CP* should be at the 85% point. Since this is very close to the *CP* used in Fig. 12, the calculation was not repeated.

The present method and Woodward's method, with *CP* at the 82% point, are in very close agreement but the span load lies slightly below that calculated by Giesing[23]. This difference may be due to the differences in mathematical models. The method of Ref. 23 simulates an infinitely long fuselage using an image system and a segmented axial doublet. An annular wing is not simulated. An annular wing, unlike a fuselage, satisfies the Kutta condition at its trailing edge. The effects of the Kutta condition diminish as the annular wing increases in length. The effects of the square root singularity diminish with increased length only if the annular wing is at zero incidence and its leading edge (inlet) is far ahead of the wing. The accuracy of the annular wing model of a fuselage is seen to increase as the fuselage length increases.

The chordwise load distributions (lifting pressure distribution) produced by Woodward's method (*CP* = 82%) and the present method are shown in Figs. 13 and 14. Figure 13 presents comparisons for lifting pressures on the wing; the agreement is excellent. Figure 14 presents the pressure difference between the upper and lower fuselage surfaces (at the same spanwise station) along the full length of the fuselage (annular wing). Again the agreement is excellent. Notice that the Kutta condition is satisfied at the trailing edge of the fuselage and that the leading edge shows a slight indication of the square root singularity that exists there.

The unsteady case has also been considered. Figure 15 shows the span load for the unsteady case oscillating at a reduced frequency of $k = 0.4$, and the span load for the steady case at $k = 0$. A calculation using a quasi-steady fuselage interference method,[26] using the image system described in Ref. 23 is included for comparison. While the correct unsteady singularities are used on the wing, the image system uses only steady flow singularities; consequently, the quasi-steady approximation produces only qualitative agreement. To improve this method, an unsteady image system as well as an unsteady segmented axial doublet should be used.

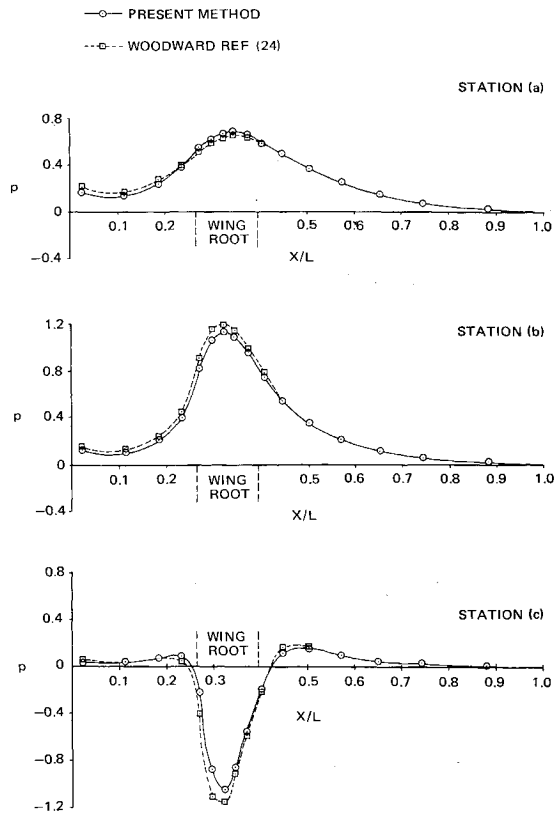

Fig. 14 Lifting pressure distributions for three fuselage stations.

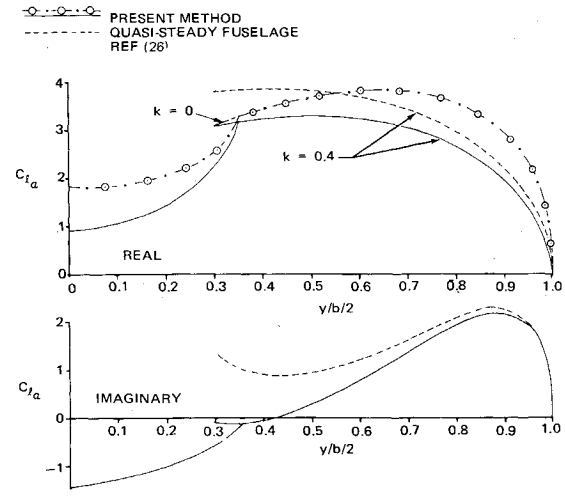

Fig. 15 Comparison of span load as calculated by quasi-steady method for wing-fuselage combination.

Wings in Ground Proximity

The present method has the capability of handling two planes of symmetry: the *x-z* and *x-y* planes. The *x-y* plane

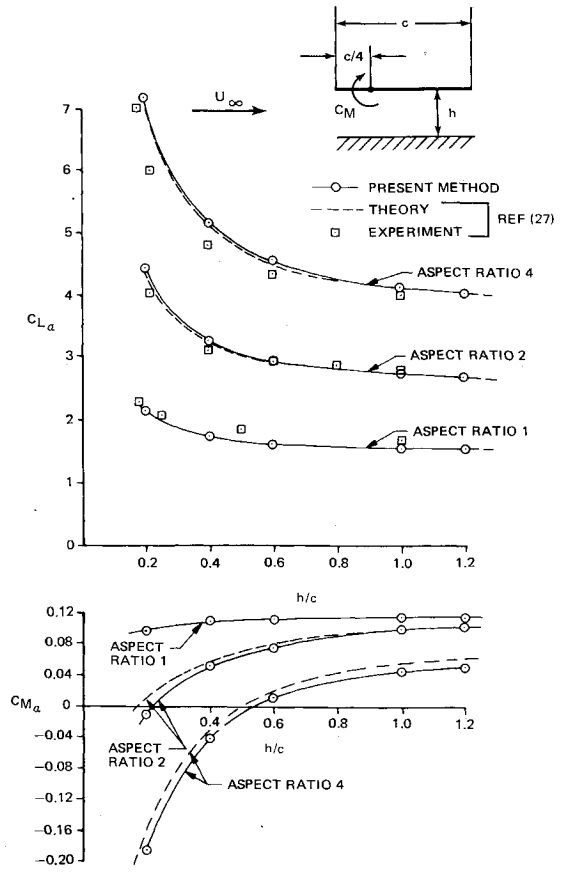

Fig. 16 Comparison of experimental and calculated steady lift-curve-slope for rectangular wings of various aspect ratios in ground effect.

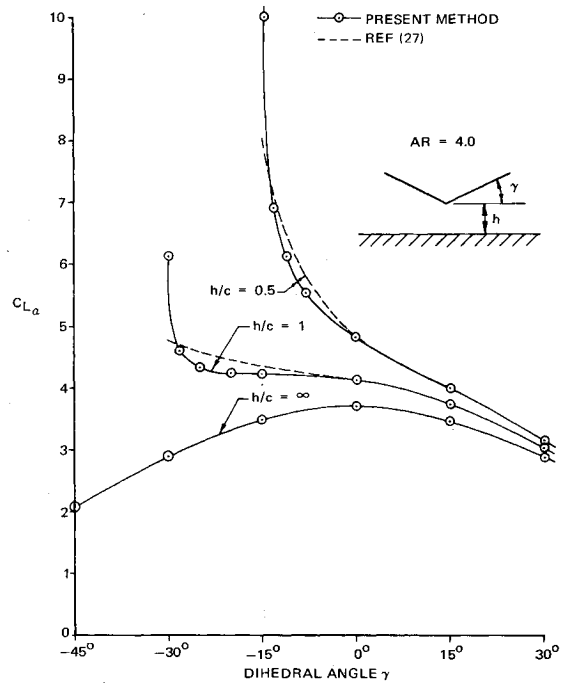

Fig. 17 Comparison of the steady lift-curve-slope as calculated by Saunders and the present method for rectangular wings in ground effect possessing various dihedral angles.

of symmetry may be used to generate the ground effect on a wing.

Saunders[27] investigated rectangular wings of various aspect ratios and dihedral angles in steady flow in the presence of the ground. Figure 16 gives a comparison of experimental and calculated lift and moment coefficients for a rectangular wing in steady incompressible flow. The lift and moment coefficients are given for wings of various aspect ratios, $AR = 1.0$, 2.0 and 4.0, as a function of the wing height above the ground plane. As seen in Fig. 16, the calculated results of Saunders are in excellent agreement with those obtained by the present method, and both calculations agree well with the experimental data taken from Refs. 28 and 29.

Figure 17 gives a comparison of the lift-curve-slope calculated by the present method and by the method of Saunders for wings with dihedral at various heights above the ground. The lift-curve-slope is shown as a function of dihedral angle for a rectangular wing with a ratio of actual semi-span to chord of 2.0 in steady incompressible flow. Saunders' results differ from those of the present method by a factor of the cosine of the dihedral angle which apparently was omitted in his calculations. Figure 17 shows that the present method and the kernel function method employed by Saunders (with C_{L_α} multiplied by $\cos\gamma$) are in good agreement, except in the case of negative dihedral where the wing tips touch the ground. When this occurs, the traditional kernel function procedure breaks down because the spanwise loading functions incorrectly force the load to zero at the wing tips.

Conclusions

Numerous correlations of the Vortex- and Doublet-Lattice Methods have been presented for a large variety of nonplanar configurations. Excellent agreement has been obtained with the results of other theoretical methods and with low-speed wind-tunnel data. Unfortunately, high-subsonic and transonic data were not available on nonplanar configurations to permit a complete correlation in the subsonic regime. The literature on experimental correlation studies now includes the planar comparisons of Refs. 3, 4, 8, 23, 26, and 30 and the present nonplanar comparisons. These correlations provide verification of the theory. While awaiting extensions of James' preliminary investigation[11] of the mathematical justification of the Lattice Methods, a mathematical foundation is regarded as a sufficient, but not a necessary condition for a practical engineering method. A higher priority item would be further correlation studies made with high subsonic and transonic pressure data obtained from wind-tunnel or flight tests. These studies would determine suitable empirical corrections for high speed and the maximum Mach number for which the method is valid. Additional correlation studies may also suggest a need for further wind-tunnel and flight test programs. Wykes[31] has investigated the use of control surfaces for load alleviation and/or mode stabilization. Such systems require accurate estimates of oscillatory hinge moment characteristics in order to specify power requirements. These can be obtained from autopilot tests in flight, but wind-tunnel measurements would provide the opportunity to investigate a greater variety of control surface configurations.

The extension of the Lattice Methods to more complicated problems is easily visualized. The use of an unsteady image system would produce an efficient method for taking into account fuselage interference effects. The same type of image system could be used to handle nacelle and external store interference. Steady axial source systems could be incorporated to generate volume effects for the fuselage, nacelles, and external stores, while unsteady axial doublet systems can be used to account for fuselage, nacelle, and store angle-of-attack effects. The loads on an entire aircraft configuration could then be determined.

Table 3 Coefficients in approximation to $1 - u/(1 + u^2)^{1/2}$

n	a_n
1	+0.24186198
2	−2.7918027
3	+24.991079
4	−111.59196
5	+271.43549
6	−305.75288
7	−41.183630
8	+545.98537
9	−644.78155
10	+328.72755
11	−64.279511

Appendix: Additional Computational Considerations

The programing algorithms for the steady downwash factors for the oblique horseshoe vortex system were taken from Ref. 4, Appendix 3. One modification was necessary in the calculation. In the case where the control point lies on the extension of the bound vortex, the calculation of the downwash factor becomes indeterminate. A series expansion for the trigonometric functions involved permits accurate calculations when the point is near the extended vortex line and leads to the proper limit (zero) when the point is on the line.

The algorithms for the incremental downwash factors for the oscillatory doublet line were obtained from Ref. 8. The downwash factor includes an integral [Ref. 8, Eqs. (6) and (7)] which, when evaluated, involves a term of the form $\zeta^{-1}\tan^{-1}c\zeta$. When the control point is near, but not at, the plane of the sending box, numerical difficulties again arise which require special consideration.¶ Two other integrals are involved in the evaluation of the kernel and can be manipulated by integrating by parts to involve integrals in the form

$$I(u_1,k_1) = \exp(ik_1u_1)\int_{u_1}^{\infty}[1 - u/(1+u^2)^{1/2}]\exp(-ik_1u)du$$

¶ A refinement of the Doublet-Lattice Method to near-coplanar configurations is given in Ref. 33.

and

$$J(u_1,k_1) = \exp(ik_1u_1)\int_{u_1}^{\infty} u[1 - u/(1 + u^2)^{1/2}]\exp(-ik_1u)du$$

A more accurate evaluation is made by using the approximation to $u/(1 + u^2)^{1/2}$ given by Laschka [Ref. 32, Eq. (53)] in place of the approximation employed in Ref. 8. The maximum error of this approximation is 0.135%. Laschka gives

$$I - u/(1 + u^2)^{1/2} \approx \sum_{n=1}^{11} a_n \exp(-ncu)$$

where $c = 0.372$ and the a_n are tabulated in Table 3.

References

[1] Falker, V. M., "The Calculation of Aerodynamic Loading on Surfaces of any Shape," R&M 1910, 1943, British Aeronautical Research Council.

[2] Rubbert, P. E., "Theoretical Characteristics of Arbitrary Wings by a Nonplanar Vortex Lattice Method," Rept. D6-9244, 1964, The Boeing Co., Seattle, Wash.

[3] Dulmovits, J., "A Lifting Surface Method for Calculating Load Distributions and the Aerodynamic Influence Coefficient Matrix for Wings in Subsonic Flow," Rept. ADR 01-02-64.1, 1964, Grumman Aircraft Engineering Corp., Bethpage, N.Y.

[4] Hedman, S. G., "Vortex Lattice Method for Calculation of Quasi-Steady State Loadings on Thin Elastic Wings," Rept. 105, Oct. 1965, Aeronautical Research Institute of Sweden.

[5] Belotserkovskii, S. M., *The Theory of Thin Wings in Subsonic Flow*, Plenum Press, N.Y., 1967.

[6] Runyan, H. L. and Woolston, D. S., "Method for Calculating the Aerodynamic Loading on an Oscillating Finite Wing in Subsonic and Sonic Flow," TR 1322, 1957, NACA.

[7] Landahl, M. T. and Stark, V. J. E., "Numerical Lifting-Surface Theory—Problems and Progress," *AIAA Journal*, Vol. 6, No. 11, Nov. 1968, pp. 2049–2060.

[8] Albano, E. and Rodden, W. P., "A Doublet-Lattice Method for Calculating Lift Distributions on Oscillating Surfaces in Subsonic Flows," *AIAA Journal*, Vol. 7, No. 2, Feb. 1969, pp. 279–285; Errata, *AIAA Journal*, Vol. 7, No. 11, Nov. 1969, p. 2192.

[9] Petkas, J. S., "Oscillatory Aerodynamic Representation Using Discrete Load Line Element (DLLE) Method," Unpublished Memorandum, Feb. 1969, Lockheed-Georgia Co., Marietta, Ga.

[10] Houbolt, J. C., "Some New Concepts in Oscillatory Lifting Surface Theory," Rept. AFFDL-TR-69-2, June 1969, U.S. Air Force Flight Dynamics Lab., Wright-Patterson Air Force Base, Ohio.

[11] James, R. M., "On the Remarkable Accuracy of the Vortex-Lattice Discretization in Thin Wing Theory," Rept DAC-67211, Feb. 1969, McDonnell Douglas Corp., Long Beach, Calif.

[12] Kalman, T. P., Rodden, W. P., and Giesing, J. P., "Aerodynamic Influence Coefficients by the Doublet Lattice Method for Interfering Nonplanar Lifting Surfaces Oscillating in a Subsonic Flow," Rept. DAC-67977, June 1969, McDonnell Douglas Corp., Long Beach, Calif.

[13] Stark, V. J. E., "Aerodynamic Forces on a Combination of a Wing and a Fin Oscillating in Subsonic Flow," Rept. TN 54, 1964, Saab Aircraft Co., Linkoping, Sweden.

[14] Davies, D. E., "Generalized Aerodynamic Forces on a T-Tail Oscillating Harmonically in Subsonic Flow," Rept. Structures 295, 1964, Royal Aircraft Establishment.

[15] Zwaan, R. J., "Calculated Results for Oscillating T-Tails in Subsonic Flow and Comparison with Experiments," Rept. MP 253, 1967, National Aerospace Lab., Amsterdam, The Netherlands.

[16] Zwaan, R. J., "Application of a Method for Estimating Pressure Distributions to an Oscillating T-Tail," Rept. TR 68048L, May 1968, National Aerospace Lab., Amsterdam, the Netherlands.

[17] Campbell, G. S., "A Finite-Step Method for the Calculation of Span Loadings of Unusual Plan Forms," RM L50L13, July 1951, NACA.

[18] Blackwell, J. A., Jr., "A Finite-Step Method for Calculation of Theoretical Load Distributions for Arbitrary Lifting-Surface Arrangements at Subsonic Speeds," TN D-5335, July 1969, NASA.

[19] Ingelmann-Sundberg, A. M. M., "Experimental Determination of Pressure Distributions on a Plane Wing with 40° Sweepback at Low Speed," Rept. KTH-AERO TN 8, 1949, Royal Institute of Technology, Stockholm, Sweden.

[20] Weber, J., and Lawford, J. A., "The Reflection Effect of Fences at Low Speeds," R&M 2977, 1956, British Aeronautical Research Council.

[21] Laschka, B., "Über die Potentialtheorie von zylindrischen rotationssymmetrischen Flügeln (Ringflügel) in kompressibler instationärer Unterschallstromung," *Zeitschrift für Flugwissenschaften*, Band 12, Heft 6, 1964, pp. 205–211.

[22] Rodden, W. P. and Giesing, J. P., "Application of Oscillatory Aerodynamic Theory for Esimation of Dynamic Stability Derivatives," *Journal of Aircraft*, Vol. 7, No. 3, May-June 1970, pp. 272–275.

[23] Giesing, J. P., "Lifting Surface Theory for Wing-Fuselage Combinations," Rept. DAC-67212, Aug. 1968, McDonnell Douglas Corp., Long Beach, Calif.

[24] Woodward, F. A., "Analysis and Design of Wing-Body Combinations at Subsonic and Supersonic Speeds," *Journal of Aircraft*, Vol. 5, No. 6, Nov.-Dec. 1968, pp. 528–534.

[25] James, R. M., "Comparison of the Woodward and Vortex Lattice Methods for a Simple Test Problem," Unpublished Memorandum, Nov. 1969, Douglas Aircraft Co., Long Beach, Calif.

[26] Stahl, B., Kalman, T. P., Giesing, J. P., and Rodden, W. P., "Aerodynamic Influence Coefficients for Oscillating Planar Lifting Surfaces by the Doublet Lattice Method for Subsonic Flows Including Quasi-Steady Fuselage Interference," Rept. DAC-67201, Oct. 1968, McDonnell Douglas Corp., Long Beach, Calif.

[27] Saunders, G. H., "Aerodynamic Characteristics of Wings in Ground Proximity," *Canadian Aeronautics and Space Journal*, June 1965, pp. 185–192.

[28] Fink, M. and Lastinger, J., "Aerodynamic Characteristics of Low-Aspect-Ratio Wings in Close Proximity to the Ground," TN D-926, July 1961, NASA.

[29] Carter, A., "Effect of Ground Proximity on the Aerodynamic Characteristics of Aspect-Ratio-1 Airfoils With and Without End Plates," TN D-970, Oct. 1961, NASA.

[30] Rodden, W. P. and Liu, D. T., "Application and Correlation of the Vortex Lattice Method of Rotor/Wing Configurations," *Journal of Aircraft*, Vol. 6, No. 4, July–Aug. 1969, p. 375.

[31] Wykes, J. H., "Structural Dynamics Stability Augmentation and Gust Alleviation of Flexible Aircraft," AIAA Paper 68-1067, Philadelphia, Pa. Oct. 1968.

[32] Laschka, B., "Zur Theorie der harmonisch schwingenden tragenden Fläche bei Unterschallstromung," *Zeitschrift für Flugwissenschaften*, Vol. 11, No. 7, July 1963, pp. 265–292.

[33] Rodden, W. P., Giesing, J. P., and Kalman, T. P., "New Developments and Application of the Subsonic Doublet—Lattice Method for Nonplanar Configurations," *AGARD Symposium, Unsteady Aerodynamics for Aeroelastic Analyses of Interfering Surfaces*, AGARD Paper No. 4, Tønsberg Oslofjorden, Nov. 3–4, 1970.